EUROPEAN ORGANIZATION FOR NUCLEAR RESEARCH

CERN/PS/DL/82-6
24 May 1982

THE TRIGGERED PSEUDO-SPARK CHAMBER AS A FAST SWITCH AND AS A HIGH-INTENSITY BEAM SOURCE

D. Bloess, I. Kamber and H. Riege
CERN, Geneva, Switzerland

G. Bittner, V. Brückner, J. Christiansen, K. Frank, W. Hartmann,
N. Lieser, Ch. Schultheiss, R. Seeböck and W. Steudtner
Physikalisches Institut der Universität Erlangen-Nürnberg,
Erlangen, Federal Republic of Germany

ABSTRACT

The pseudo-spark phenomenon opens a wide field of applications in accelerator, high-voltage, and high-current handling technology. A basic model is described which explains the initialization and the growth of the pseudo-spark discharge process in two phases. The discharge characteristics of single-gap and multigap pseudo-spark chambers have been investigated. In both types of chambers the breakdown can be triggered easily. With single-gap chambers one can switch voltages in the kV range and currents in the kA range. Multigap chambers generate pulsed, pinched electron beams with peak currents up to 5 kA with FWHM of 2 ns to 20 ns and densities greater than 10^6 A/cm^2. With the aid of these intense electron beams, highly charged ions such as Kr^{13+} have been produced. From multigap chambers one can also extract well-focused ion beams. The experimental results are compared with a model describing the pseudo-spark phenomenon. The applications of the pseudo-spark chamber as a triggerable, fast, high-voltage, high-current switch and as a pulsed, high-density electron- and ion-beam source are discussed.

(To be submitted to Nuclear Instruments and Methods)

1. INTRODUCTION

The electrical breakdown in gases is described by Paschen's law $U_B = f(pd)$. Figure 1 shows a typical breakdown curve characterized by a nearly linear rise at (p•d)-values above 25 to 40 mbar•mm, a minimum around 7 to 13 mbar•mm and a steep rise below the minimum. Breakdown below 10^{-4} mbar•mm is called vacuum breakdown. Different physical mechanisms govern the discharge in the different regions of the Paschen curve. At high pressures electron avalanches expand very fast into streamer discharges. Near the Paschen minimum the main process is glow discharge based on the ionization by electrons and on the creation of electrons from electrode surfaces through ion impact. Vacuum breakdown is mainly a surface phenomenon, where the carriers are liberated by desorption, ion-impact, and field emission, and then undergo acceleration and charge multiplication.

The breakdown in the range between the Paschen minimum and the region of vacuum breakdown induced in a specific geometrical configuration is the subject of this paper. Breakdown at low pressure has been studied, for example, by Townsend [1], Dempster [2], McClure et al. [3-5], Parker et al. [6-10], and Lauer et al. [11]. High-density electron and ion beams have been observed by Christiansen et al. [12] in a discharge chamber composed of metal electrodes with a centre hole held by a surrounding insulating wall (fig. 2). The discharge in such a chamber has some similarity to a high-pressure spark discharge. Since its mechanism, however, differs from the high-pressure discharge mechanism, the breakdown in such a chamber is called a "pseudo-spark". The pseudo-spark can build up in less than 5 ns with currents which may extend into the kA region. Pinched electron beams with current densities greater than 10^6 A/cm^2 leave the pseudo-spark chambers. The self-capacitance of the chamber can be charged to a constant voltage and discharged spontaneously, or it can be pulsed from an external high-voltage pulse generator. In this paper we mainly report on experiments performed with chambers which are charged to constant voltage and which are ignited with the aid of an external trigger pulse. These studies support the practical development of high-voltage, high-current switches and pulsed ion- and electron-beam sources. In

addition they are helpful for the fundamental exploration of the underlying discharge mechanisms.

2. BASIC MODEL OF THE PSEUDO-SPARK DISCHARGE

A model has been established [13] which describes the initialization of a pseudo-spark discharge in the case of a single-gap chamber (fig. 3). From experimental observations one can conclude that the pseudo-spark discharge builds up in two phases: a pre-breakdown phase and the proper breakdown.

i) During the pre-breakdown phase, negative and positive charges are created by ionization acts between anode and cathode. Whereas the electrons are immediately captured by the anode, the positive carriers fly towards the cathode and mainly through the cathode hole into the nearly field-free space behind. There they form a positive space charge which we call the virtual anode.

ii) During the second phase, a fast carrier multiplication process inside the virtual anode leads to a high plasma density. The rather slow growth of the virtual anode is followed now by a very fast breakdown discharging the whole system. Axially an intense well-focused electron beam is formed and accelerated towards the anode. There the electron beam leaves the chamber through the anode hole. The electron current is accompanied by an ion current partly striking the cathode and partly forming an ion beam which leaves the chamber through the cathode hole.

It is well known that the ionization by electrons, which is the dominant process in Raether's spark mechanism [14], plays only a negligible role for the charge carrier multiplication in the pressure region of the pseudo-spark left of the Paschen minimum. Here the important multiplication processes are ionization by ions and neutrals as well as by back-scattered electrons [1-11].

Back scattering of electrons from the anode and liberation of electrons by direct ion- and neutral-impact on the cathode (γ-effect) can play only a minor role because of the central holes in both electrodes. Fast neutral particles, formed by recombination of ions and electrons moving to the cathode, do not contribute to the

build-up of the virtual anode. It seems that the major multiplication process is based on the formation of ion avalanches. This hypothesis is supported by experimental observations and theoretical considerations, according to which ionization by ions can take place already at energies as low as 100 eV [15-17]. On their way to the cathode, positive carriers created between the electrodes can multiply by a factor of 5 to 10. The avalanches of positive ions then move through the cathode hole, expand owing to scattering and electrical defocusing, and form with their positive space charge the virtual anode. The build-up of this virtual anode is essential for the start of the second phase and the final breakdown.

The positive space charge acts as a potential drain for electrons which have been formed by the γ-effect of ions inside and behind the cathode. Experimental observations show that the virtual anode has typically a potential of several hundred volts [13]. Therefore the attracted electrons have an energy near the maximum of their ionization probability. They may rapidly further increase the ionization within the virtual anode and so create the condition for the rapid breakdown of the chamber.

The field distribution between the virtual anode, the cathode, and the anode favours the formation of an electron beam directed towards the anode. The ion flux towards the cathode prevents the build-up of a positive over-charge in the virtual anode and, at the same time, forms the source of new γ-electrons. The pseudo-spark discharge may transform into a d.c. discharge, when the formation of the virtual anode is inhibited, for example by closing the cathode hole.

The measured intense electron current densities require correspondingly high ion current densities from the virtual anode to the cathode. An unbalanced electron flux would otherwise charge the virtual anode to an extremely high positive potential value. The high ion flux is generated by the high electric field in the Debye sheath at the plasma envelope between the virtual anode and the cathode. The plasma sheath has a thickness of the order of the Debye length

$$\lambda_D = \left(\frac{\varepsilon_0 \, k \, T_{el}}{e^2 \, n_{el}} \right)^{\frac{1}{2}} , \qquad (1)$$

where k = Boltzmann constant, T_{el} = mean electron temperature, n_{el} = electron density, ε_0 = dielectric constant, and e = elementary charge.

Across an extraction length of 2.5 λ_D the positive potential U_{VA} of the virtual anode drops down partially by

$$U_D = \frac{kT_{el}}{2e} . \tag{2}$$

Therefore the ion current density j_i passing through the Debye layer is given by Bohm's equation

$$j_i = a\, en_{el} \left(\frac{kT_{el}}{m_i} \right)^{\frac{1}{2}} , \tag{3}$$

where a is of the order of 1, m_i the ion mass, and U_D acts as the extraction potential. The current density given by eq. (3), which is a modified Langmuir-Child equation, can greatly exceed the normal Langmuir-Child space-charge limit.

The pseudo-spark model described for a two-electrode system can be extended to multi-electrode chambers. Multiple electrodes electrostatically focus better the ion current in the pre-breakdown phase and the electron beam in the breakdown moment. This additional focusing effect enables the formation of pinched electron beams with current densities above 10^6 A/cm^2.

3. EXPERIMENTAL RESULTS

Previously the experiments have been mainly carried out with pseudo-spark chambers charged to constant voltage and breaking down in the spontaneous breakdown mode. A trigger mechanism has been developed for pseudo-spark chambers charged from a d.c. high-voltage power supply. The advantages of triggering are obvious, whenever one envisages using pseudo-spark chambers as switches and pulsed beam sources. Only precise triggering enables synchronization with external systems such as pulse generators or post-acceleration systems.

From the model described in the previous section, it follows that efficient triggering should be possible, utilizing the fact that the main breakdown always starts from the cathode. An essential feature of the pseudo-spark is that a plasma is required in the cathode region for breakdown to occur. Thus a trigger

pulse has to be applied just at the cathode where it generates, for example by surface flash-over, a local plasma which then grows into a pseudo-spark.

3.1 Single-gap chamber

3.1.1 Experimental chamber

The simplest system in which a pseudo-spark occurs is a single-gap chamber consisting of an anode and a cathode each with a centre hole (fig. 3). To study the breakdown phenomena in detail, an experimental chamber was constructed with metal plates and insulating rings which could easily be put together and connected electrically in the desired way. The whole set-up was mounted in a vacuum tank to avoid external flash-over. Discharge tests were performed, either with the self-capacitance of the chamber charged to a constant voltage or with added external capacitors or pulse cables.

Figure 4 shows the chamber configuration and the electrical circuitry which has been used for static and triggered breakdown tests. The thin metal disc together with the lower ground electrode (cathode) form the trigger. Both are separated by an insulating disc. Additional discs below the ground electrode serve either as collector plates, like a Faraday cup, to capture the beam current passing through the hole of the ground electrode, or as blocking potential plates acting upon the virtual anode, thereby increasing the main breakdown voltage. Cables of 50 Ω impedance and of variable length are charged through a load resistor and discharged via a 50 Ω resistor through the chamber to ground. Current measurements are made on a 1 Ω shunt resistor between the chamber cathode and earth.

The static breakdown voltage of the chamber filled with nitrogen and without trigger and blocking potential is given as a function of pressure in fig. 5 ("Paschen curve"). Polarity reversal does not lead to the same result since the chamber is not symmetrical.

As mentioned above, a positive or negative potential on the metal plate below the cathode (ground electrode) increases the breakdown voltage by 50%. To raise

the main charging voltage from 10 kV to 15 kV, a positive or negative blocking voltage of only 40 V is required. This effect was first used to trigger the breakdown of the chamber. The working point is then placed between the increased breakdown voltage curve (3) and the natural breakdown curve without blocking potential (1) (fig. 5). By cancelling momentarily the d.c. blocking potential with a trigger pulse of inverse polarity, breakdown can be achieved. However, the required trigger pulse length is of the order of 1 ms and the delay and jitter of the main breakdown are of the order of microseconds.

Therefore an attempt was made to trigger the breakdown of the chamber with a 2 kV pulse applied to the trigger plate and the ground electrode across a small concentric insulating gap (fig. 4). It appears that whenever the trigger gap breaks down the main gap follows within 1 ns. One can hardly detect any delay and jitter between the breakdown of the trigger and the main gap. The over-all delay and jitter of the chamber is determined by the breakdown characteristics of the trigger gap and the trigger circuit parameters.

The trigger effect occurs over the whole range between the spontaneous breakdown curve and charging voltages down to 100 V. No lower pressure limit could be observed with this chamber at voltages above 8 kV. At the lowest applied pressures of 2×10^{-3} mbar triggering still works for the gases H_2, D_2, He, N_2, and Kr. An equally large trigger range is observed for reversed polarity, hence for negative main voltage and triggering now at the anode. However, in the latter case a considerable delay between trigger gap and main gap breakdown is measured (figs. 6a and b). Figure 7 shows the delay time between the anode trigger breakdown and the main breakdown for N_2, H_2, He, and Kr, as a function of pressure.

For switching applications, it is interesting to know the internal resistance of the chamber after breakdown as a function of time. Discharges of 50 Ω cables up to 4 μs length via a 50 Ω resistor were made at 15 kV charging voltage. The current was measured across the 1 Ω shunt resistor. The internal resistance drops below 0.1 Ω within a few ns after breakdown. With pulse durations up to 4 μs no gas exhaustion has been observed. The total current splits into two components: one

striking directly the ground electrode, the other passing as a charged particle beam through the centre hole and hitting the collector plate below the ground electrode. Both currents have been measured separately as functions of time and shunt resistor value for both polarities as shown in fig. 8a. At any instant the sum of both currents corresponds to the measured total current. The current distribution on the flat top of the pulse (1 μs after breakdown) depends in all cases only upon the resistor ratios in series with the corresponding electrodes. In the leading part of the pulse, the current redistribution is influenced strongly by the polarity. If an ion beam passes through the hole of the ground electrode (cathode), it arrives at the collector electrode after a delay of several 100 ns, depending on pressure and gas type. In the meantime the cathode takes the total current (figs. 8b and c). With reversed polarity and electrons passing through the ground-electrode centre hole, one observes immediately after breakdown a current distribution corresponding to the ratio of the two measuring resistors (figs. 8d and e).

3.1.2 *The single-gap pseudo-spark chamber as a switch*

The main features of a good, fast, high-voltage, high-current switch, such as a thyratron, are fast rise-time, negligible internal resistance, easy ignition by an external trigger, low delay-time, low jitter, and fast recovery-time. The results obtained with the experimental single-gap chamber show that a pseudo-spark switch could fulfil these requirements. In order to get an idea about long-range reliability and related material problems, a simple prototype switch was built as shown in figs. 9a and b. The pseudo-spark switch could be disassembled easily and its components could be exchanged. At first a concentric 0.1 mm insulating gap inside the cathode served as the trigger source. The chamber was incorporated into a 25 Ω impedance cable pulse generator (maximum charging voltage 30 kV), the scheme of which is given in fig. 10. By triggering the pseudo-spark switch and the thyratron at the other end of the main pulse cable with two separately delayed trigger pulses, rectangular pulses of variable length are generated. In these

tests nitrogen at a pressure of 0.1 mb was used in the chamber. At the beginning of the operational test the current rise-time of the pseudo-spark switch was about 10 ns, mainly determined by the geometry of the construction (figs. 11a and b). The jitter was measured between the low-voltage input pulse to the trigger unit 1 (also external trigger for the oscilloscope) and the main current pulse signal on a 0.2 Ω shunt resistor between the switch and ground (see fig. 10). With a new trigger insulator embedded between tungsten electrodes, the over-all jitter of the pseudo-spark gap is less than ±1 ns.

After two million pulses the jitter was still smaller than ±2 ns. The switch finally worked up to 5.5 million pulses of 1 to 2 μs length, at charging voltages between 20 and 30 kV, and at pulse repetition rates of 1 to 20 Hz. Then, owing to the presence of organic material inside the chamber volume, carbon deposit on the main insulator led to a final short circuit of the main gap. A maximum charging voltage of 55 kV was supported by the pseudo-spark switch in vacuum. Above this level breakdown occurred by flash-over on the external nylon screws (fig. 9).

Figure 12a shows the scheme of a double-gap chamber with two trigger electrodes. This device allows the generation of rectangular pulses of variable length from a storage cable similarly to the 25 Ω pulse generator with the thyratron and the pseudo-spark gap described above. However, the two switches are now combined in one single pseudo-spark chamber. There is no evidence for mutual interference when one gap is pulsed and the other not. Figure 12b gives the output pulses with different delays between the two triggers, measured on a simple current pick-up.

3.2 Multigap chambers

3.2.1 Electron beam source

Although with a single-gap pseudo-spark chamber electron and ion beams can be observed, the pinched electron beams can only be extracted from multigap chambers. The optimum chamber configuration for each type of beam is different and determined by the efficiency with which the stored energy is converted into ion- or electron-beam energy. High efficiencies of up to 60% have been found for electron-beam

generation. Well-pinched electron beams can be produced with chambers having more than 10 cells and with voltages of typically 50 kV across the whole chamber length (figs. 2 and 13a). The chambers are either made of metal and glass discs or metal and ceramic discs. They are either soldered together or pressed together with the aid of insulating bars reinforced with glass fibres. Figure 13b shows such a chamber fully assembled in a vacuum tank. The experiments were partly performed by discharging the self capacitance of the chamber. Whenever higher and longer beam current pulses were required, the necessary charge was provided by fixing external high-voltage capacitors at the end electrodes of the pseudo-spark chamber.

The results obtained by triggering single-gap chambers suggested trying external triggering also with a multigap chamber. When operating the latter in a "free running" mode one has almost no control over its pulse repetition rate. In this case also the shot-to-shot variations in beam-current amplitude and waveform are considerable. This can be improved by discharging the chamber at settled conditions of pressure and voltage with a method similar to the one used in single-gap chambers. A thin insulating foil embedded in the ground electrode of the chamber forms the trigger gap (fig. 13a). The multigap chamber can be triggered efficiently when the ground electrode is the cathode. However, for the purpose of observation, one wants to extract the electron beam on the ground side, so that the ground electrode has to be the anode. In the latter case triggering is much less efficient in terms of jitter, delay, and trigger range. Nevertheless stable triggering at the anode can be achieved within a limited pressure and voltage range for most gases.

Figures 14a, b, and c give some typical beam-current waveforms measured with a wide-band current transformer [18] (t_{rise} = 0.2 ns) placed about 80 mm from the exit of the pseudo-spark chamber. In front of the transformer and at the interface to the high vacuum in the tank target foils have been used. These foils served, on the one hand, to separate the low-pressure region of the chamber from the surrounding vacuum and, on the other hand, as witness plates for profile and current density measurements. Figure 15 shows a typical hole drilled by a series of beam pulses through a 300 μm brass foil.

A current density of more than 10^6 A/cm^2 results from the measured current amplitudes of up to 80 A, obtained without external capacitors, and from the diameter of the drilled holes (typically 50 to 100 µm). The very high beam currents in the kA range (fig. 14c) generated with an external capacitance of 0.8 nF seem to blow up outside the chamber. A single pulse of 2 kA peak amplitude drills a hole of 2 mm diameter through a 5 µm Al foil at 80 mm from the exit of the chamber.

Though the pseudo-spark effect is a general phenomenon observed in all gases, the influence of the type of gas on the electron-beam formation is quite important. We observed well pinched beams in nitrogen and heavier gases. With deuterium and hydrogen the drilling effect of the electron beam seems to be weaker, the pinching less good, and the beam current amplitudes much smaller.

3.2.2 Ion-beam source

The properties of the ion beam generated on the cathode side of the pseudo-spark chamber have been studied in various experiments.

The diameter of the ion beam in low-pressure gas was determined as a function of distance from the cathode by drilling holes through thin plastic foils [12] (fig. 16). A well-focused, high-current (30 A) ion-beam pulse of small diameter is obtained when injecting the ion beam from a pseudo-spark discharge into a focusing post-acceleration geometry (fig. 17). Such a beam drills holes of 30 µm diameter through copper foils of 100 µm thickness.

The energy spread of the ions has been measured with a retarding field-analysing device. The beam contains a high number of low-energy ions which have less than 20% of the energy corresponding to the charging voltage.

The ion beam has been analysed after its drift through a low-pressure gas region and its ejection into high vacuum through a small aperture. Photographs with a Thomson parabola spectrometer showed only ions of charge state +1. Nevertheless, in the virtual anode, ions with higher charge states can be observed by means of optical spectroscopy. However, by drifting through the low-pressure gas they will recombine. The gas region behind the cathode is, on the other hand, necessary for the formation of the pseudo-spark discharge.

For the production of highly charged ions a different method was used. The pinched, high-density electron beam interacts with the residual gas in the anode region. Highly charged ions are produced and extracted into high vacuum by an extraction electrode. Charge states up to Kr^{13+} could be observed with a Thomson spectrometer [19] (fig. 18).

4. DISCUSSION

4.1 Comparison between test results and the pseudo-spark model

The results of the measurements will now be discussed in the frame of the model presented in Section 2. The observed trigger phenomena support the idea that the discharge takes place in two stages. When the trigger pulse is applied at the cathode, the charge carriers are generated by the trigger spark directly in the cathode region. The pseudo-spark discharge then occurs immediately in a very wide pressure range without measurable delay (see fig. 6a). Apparently phase 1 of the discharge is omitted and the assumption that the final breakdown starts from the cathode is confirmed.

If the trigger is applied at the anode a delay between trigger breakdown and main breakdown is measured which roughly corresponds to the ion transit time from the anode to the cathode. The delay effect is also a clear sign for the breakdown starting at the cathode.

The total delay-time is composed of the time of flight of the ions (phase 1) and the build-up time for charge multiplication in the virtual anode (phase 2). The latter delay is gas- and pressure-dependent (fig. 7). In heavier gases, with higher nuclear charge (more electrons per molecule), shorter build-up times are observed. The build-up time increases at lower pressure. Both observations confirm that the charge-multiplication process within the virtual anode is mainly based on ionization by electrons.

Besides the direct triggering of the discharge, it is possible to inhibit the breakdown by a blocking potential (±1 V to ±40 V) applied to an electrode behind

the cathode (fig. 4). The effect of the blocking voltage, which is very small, compared to the main charging voltage, can only be explained by a sucking off or pushing away of slow electrons, which are the basis of charge multiplication in the virtual anode region during phase 2.

The two-stage model describes the pseudo-spark discharge only up to the final breakdown. The separate measurements of the currents in the single-gap chamber, which flow either directly to the main electrodes or through the centre hole to the collector electrode (fig. 8), allow one nevertheless to reach conclusions on the second phase of the discharge. An ion-beam current flows through the cathode hole to the capture electrode with a time delay which is proportional to the square root of the ion mass and which equals the time of flight from the main gap to the capture plate. During the same time the current striking the cathode drops down to a value corresponding to the shunt resistor ratio on both electrodes. This again is a demonstration that the discharge starts at the cathode.

4.2 Comparison of the pseudo-spark switch with existing switches

The pseudo-spark switch, described in Section 3.1.2, was the first one ever built. Its characteristics and potential future capabilities will now be compared with those of conventional switches such as thyratrons and spark gaps.

With a relatively small trigger pulse the switch can be turned on in almost the whole range below its proper "Paschen curve". With such a large trigger range it is superior to spark gaps. The current rise-time is comparable to that of spark gaps and is better than that of thyratrons mainly owing to geometrical reasons such as the smaller size. The jitter is comparable to thyratron jitter and better than spark-gap jitter. No delay exists between trigger and main breakdown when cathode triggering is used. Unlike with thyratrons, current reversals can be tolerated without any problem. Pseudo-spark switches can be built for either positive or negative polarity.

The same switch can be used for both polarities provided the delay when triggering at the anode can be accepted. Owing to a very short recovery time, high repetition rates are possible. Multigap chambers have been pulsed in

free-running mode at several MHz. The cathode of the pseudo-spark switch does not need heating like thyratron cathodes. The high-current and high-voltage limits are not yet known but there are indications that one can switch currents and powers comparable to or higher than those in spark gaps, and high voltages above one hundred kV. Because of the low gas pressure, the small radiation sensitivity of the pseudo-spark switch allows its operation in high-radiation environments such as accelerators, fission and fusion reactors. A further advantage of the pseudo-spark switch is its geometry. Unlike in spark gaps and thyratrons the discharge takes place in a hole, and energetic particles do not primarily hit essential elements such as electrodes or grids. They are transported into the regions behind the electrodes where their damaging effect can be easily controlled.

The use of inorganic materials for main-gap and trigger-gap insulation and of tungsten at all places which are hit by particle beams will prolong the lifetime of a pseudo-spark switch. The main problem of this switch is the trigger construction when long lifetime, high switching power, negligible jitter, and constant delay are required at the same time. Finally, it should be mentioned that the simple construction allows the building of a switch at low cost.

4.3 Applications for triggerable electron- and ion-beam sources

The interesting features of the pseudo-spark chamber e.g. compactness, easy handling, high electric field strength, capability of producing electron currents of high density and excellent spatial confinement, could find application in accelerator beam sources and in future accelerator structures. However, the high currents and current densities require new post-acceleration principles and techniques. The transport of such currents through the ultra-high vacuum of conventional accelerators is impossible owing to immediate disintegration of the beam by space-charge forces. This can easily be observed with the ion beam in the cathode region and with the electron beam when it is directly ejected at the anode into the vacuum.

The possibility of maintaining electric fields of up to 10^8 V/m in the gas-filled chambers and the excellent transport properties of intensive particle beams in low-pressure gas suggest the application of such structures for particle acceleration. The practical realization of post-acceleration is certainly a problem. The post-acceleration along a gas-filled path and the use of differentially pumped gas cells at suitable distances for repeated reformation of the beam needs to be investigated. Particle and energy loss, as well as the conservation of the good spatial confinement, have to be optimized. Success in this field could lead to small and compact "microaccelerators". The source of highly charged ions [19] described in Section 3.2.2 can already be applied in existing accelerators.

As mentioned in Section 4.1, triggering of the pseudo-spark discharge at the cathode is superior to anode triggering also in multigap chambers. Triggering from the anode is possible when one accepts a delay between trigger and main breakdwon as well as a limited pressure and voltage operating range. Whenever synchronization is necessary between the pseudo-spark chamber and following post-acceleration elements, cathode triggering is essential, but it may have to be performed on the HV electrode. The usual bunching structures in low-energy accelerators are probably not needed, since the particles leave the chamber already in the form of bunches. All that has been said above about triggering is valid also for ion-beam generation, which works with all noble and most molecular gases. As described in Section 3.2 immediate post-acceleration and focusing of the ion beam leaving the discharge chamber are necessary in order to maintain the spatial concentration of the low-energy ion beam.

5. CONCLUSIONS

The basic results of the measurements described in this paper are in good agreement with the predictions of the pseudo-spark model. The model needs refinement and extension into the breakdown phase proper. The formation and the transport of the intense charged-particle beams require more detailed explanation.

The single-gap pseudo-spark chamber has proved to be a candidate for a high-voltage, high-current switch at a low price. Switching of currents in the kA region and of voltages above 100 kV seems possible.

As a cheap and simple electron source, the multigap chamber can generate beams of more than 10^6 A/cm^2 current density. Apart from many other applications, electron beams with such qualities could be used for collective acceleration of ions.

The pseudo-spark chamber may work as a low-energy injector of light and heavier ions into post-acceleration systems such as MEQALACS [20] and radio-frequency quadrupoles [21].

Acknowledgements

We wish to express our thanks to P. Billault, who, with his skilled mechanical work and high motivation, contributed considerably to the success of our research. It is a pleasure to mention the help of A. Dind and M. Van Gulik in designing pseudo-spark chambers and setting up experiments. We are particularly indebted to X.L. Jiang for fruitful discussions.

REFERENCES

[1] J.S. Townsend, Philos. Mag. 6 (1903) 389 and 598.

[2] A.J. Dempster, Phys. Rev. 46 (1934) 728.

[3] G.W. McClure, Phys. Rev. 124 (1961) 969.

[4] G.W. McClure and K.D. Granzow, Phys. Rev. 125 (1962) 3.

[5] K.D. Granzow and G.W. McClure, Phys. Rev. 125 (1962) 1792.

[6] A.B. Parker and P.C. Johnson, Proc. R. Soc. London Ser. A, 325 (1971) 511.

[7] J.D. Pace and A.B. Parker, J. Phys. D6 (1973) 1525.

[8] A.B. Parker and J.D. Pace, Proc. 11th Int. Conf. on Phenomena in Ionized Gases, Prague, 1973 (Czechoslovak Academy of Sciences, Prague, 1973), p. 102.

[9] J.D. Pace and A.B. Parker, Proc. 3rd Int. Conf. on Gas Discharges, IEE, London, 1974 (IEE, London, 1974), p. 91.

[10] D. Bhasavanich and A.B. Parker, Proc. R. Soc. London Ser. A 358 (1977) 385.

[11] E.J. Lauer, S.S. Yu and D.M. Cox, Phys. Rev. A 23 (1981) 2250.

[12] J. Christiansen and C. Schultheiss, Z. Phys. A 290 (1979) 35.

[13] W. Hartmann, G. Bittner, V. Brückner, J. Christiansen, K. Frank, C. Schultheiss und W. Steudtner, Untersuchungen zum Mechanismus der Pseudofunkenendladung, Forschungsbericht, Physikalisches Institut, Universität Erlangen-Nürnberg, Nr. 8, 1981.

[14] H. Raether, Ergebn. exakt. Naturwiss. 33 (1961) 175.

[15] H.B. Gilbody and J.B. Hasted, Proc. R. Soc. London Ser. A 240 (1957) 382.

[16] J.S. Briggs and J.H. Macek, J. Phys. B6 (1973) 982.

[17] K. Taulbjorg, J.S. Briggs and J. Vaaber, J. Phys. B9 (1976) 1351.

[18] J.M. Anderson, Rev. Sci. Instrum. 42 (1971) 915.

[19] G. Bittner, J. Christiansen and N. Lieser, to be published in Appl. Phys. B.

[20] A.W. Maschke, BNL-51029, UC-28, Brookhaven Nat. Lab., 1979.

[21] R.H. Stokes, K.R. Crandall, R.W. Hamm, F.J. Humphry, R.A. Jameson, E.A. Knapp, J.M. Potter, G.W. Rodenz, J.E. Stovall, D.A. Swenson, and T.P. Wangler, Proc. XIth Int. Conf. on High-Energy Accelerators, CERN, Geneva, 1980 (Experimentia: Supplement 40, 1981), p. 399.

Figure captions

Fig. 1 : Typical Paschen curve.

Fig. 2 : Basic scheme of a multigap pseudo-spark chamber.

Fig. 3 : Basic scheme of a single-gap pseudo-spark chamber.

Fig. 4 : Scheme of the experimental pseudo-spark chamber.

Fig. 5 : Characteristic breakdown voltage U_B of the experimental chamber as a function of pressure p for positive (1) and negative (2) polarity. With a blocking potential ≥ 40 V the positive breakdown voltage can be raised by 50% (3); $d_{eff} \approx 7.5$ mm.

Fig. 6 : Delay t_D between the trigger- and the main-gap breakdown for positive (a) and negative (b) charging and trigger voltage polarity.

Fig. 7 : Delay-time t_D between the trigger and the main-gap breakdown as a function of pressure in the case of triggering at the anode.

Fig. 8 : Measurement of the distribution of currents striking the ground electrode (shunt S1) and the beam-collector electrode (shunt S2). a) Principle of measurement. b) Current via S1 with positive charging voltage. c) Ion-beam current via S2. d) Current via S1 with negative polarity. e) Electron-beam current via S2.

Fig. 9 : Prototype of a pseudo-spark switch. a) Side view. b) Principle of construction.

Fig. 10 : Circuit diagram of the test set-up for the pseudo-spark switch.

Fig. 11 : Rise-time of the thyratron (a) and the pseudo-spark switch (b) in the test pulse generator. Scale: 10 ns/div.

Fig. 12 : Variable-width square-pulse generator built with a double-gap pseudo-spark switch. a) Principle of the pulse generator. b) Output pulses of variable length measured on SR1 or SR2. Charging voltage 8 kV.

Fig. 13 : Scheme (a) and view (b) of a multigap pseudo-spark chamber with trigger gap and mounted in a vacuum tank.

Fig. 14 : Electron-beam current waveforms measured with a wide-band transformer 100 mm from the exit of the chamber: a), b) with self-capacitance of the chamber only; c) with 750 pF external capacitance.

Fig. 15 : Hole drilled through a 300 μm brass foil by a series of electron-beam pulses.

Fig. 16 : Ion-beam diameter as a function of the distance from the cathode.

Fig. 17 : Pseudo-spark chamber for the generation and post-acceleration of a concentrated ion beam.

Fig. 18 : Typical krypton parabola-spectrum. The highest still visible charge state (upper arrow) is Kr^{13+}. The lower arrow marks Kr^{+}. Between them the other charge states can be identified. Also visible are ions from the chamber material and from impurities. The black spot on the lower left side is the origin of the coordinate system. The x-axis is obtained by switching off the magnetic field.

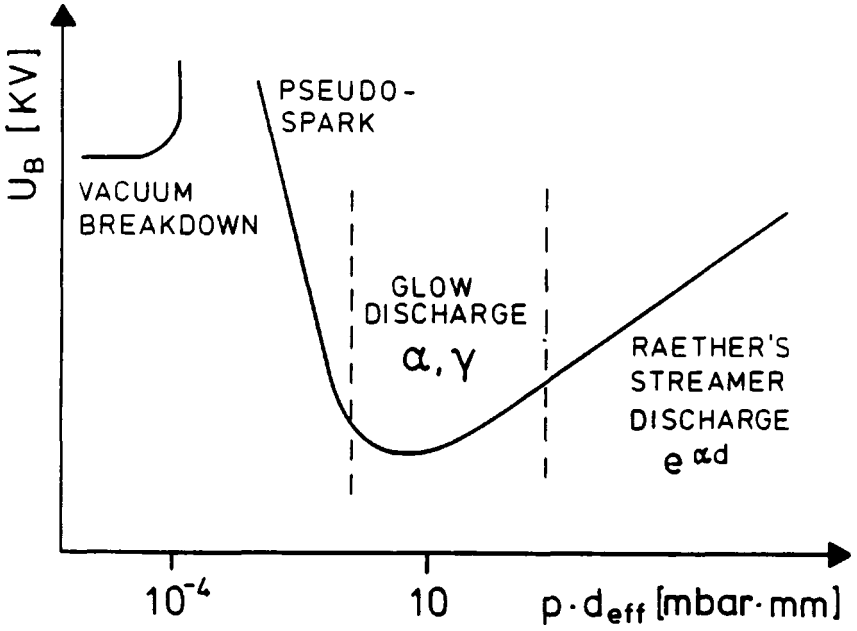

Fig. 1

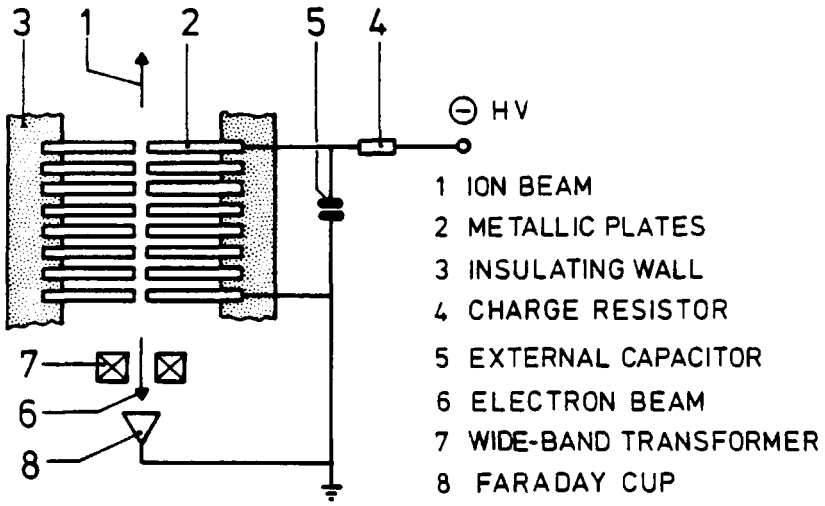

Fig. 2

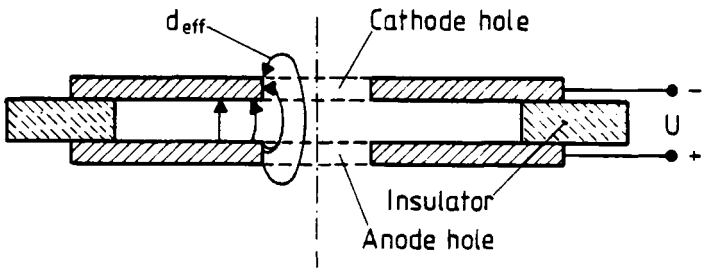

Fig. 3

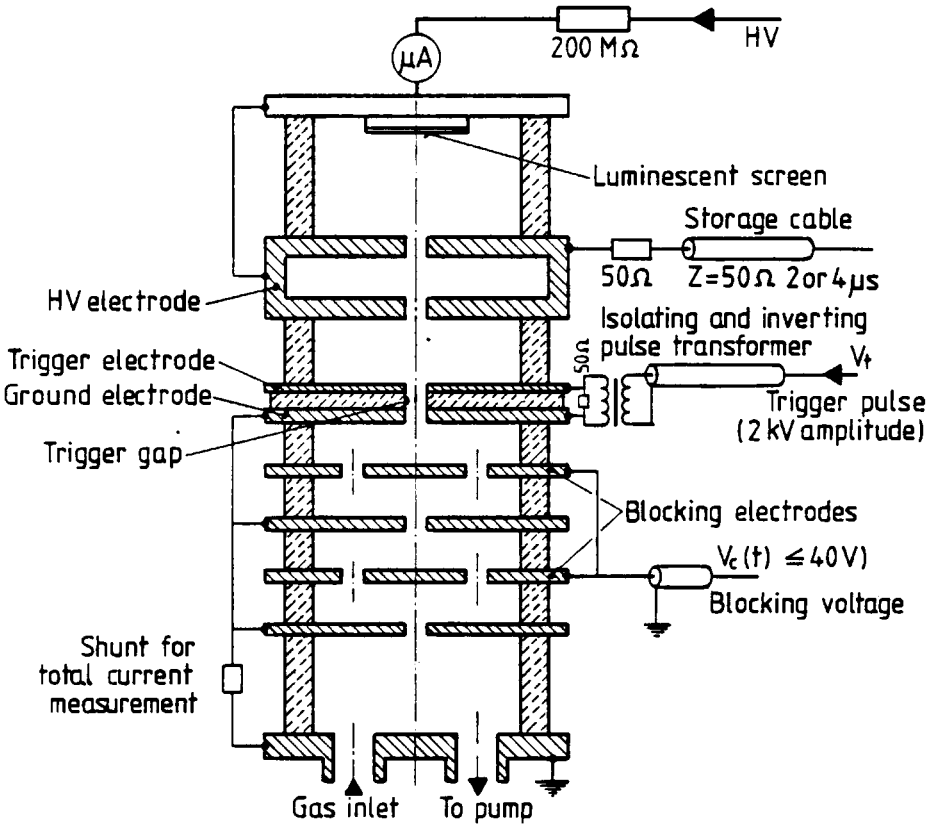
μA
200 MΩ
HV
Luminescent screen
Storage cable
50Ω
Z=50Ω 2or4μs
HV electrode
Isolating and inverting
pulse transformer
50Ω
Vt
Trigger electrode
Ground electrode
Trigger pulse
(2 kV amplitude)
Trigger gap
Blocking electrodes
Vc(t) ≤40V)
Blocking voltage
Shunt for
total current
measurement
Gas inlet
To pump

Fig. 4

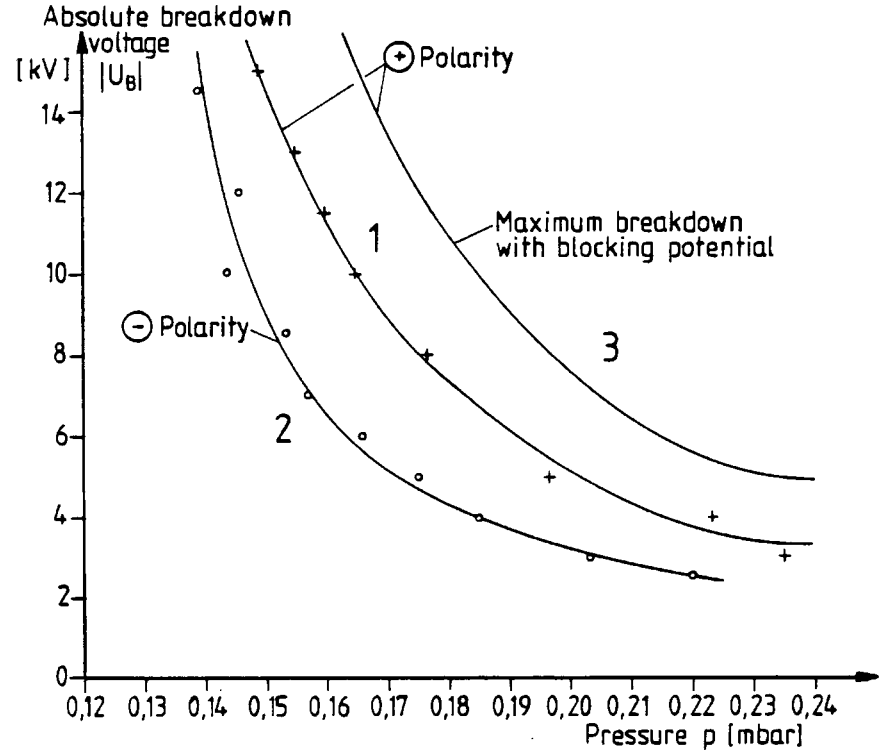
Absolute breakdown
voltage
[kV] |UB|
Polarity
Maximum breakdown
with blocking potential
1
2
3
Polarity
14
12
10
8
6
4
2
0
0,12 0,13 0,14 0,15 0,16 0,17 0,18 0,19 0,20 0,21 0,22 0,23 0,24
Pressure p [mbar]

Fig. 5

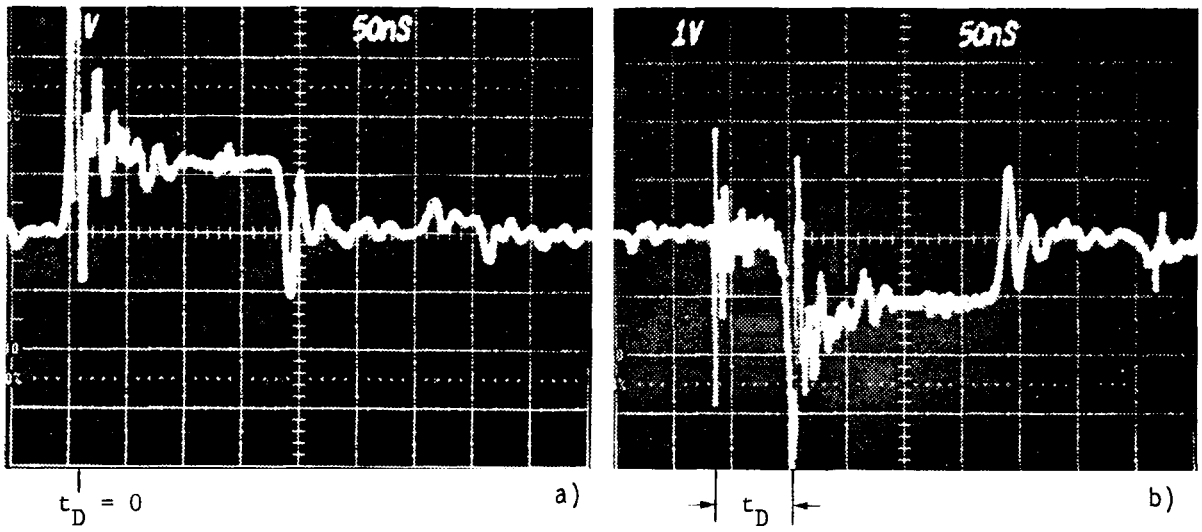
1V
50nS
t_D = 0
a)
1V
50nS
t_D
b)

Fig. 6

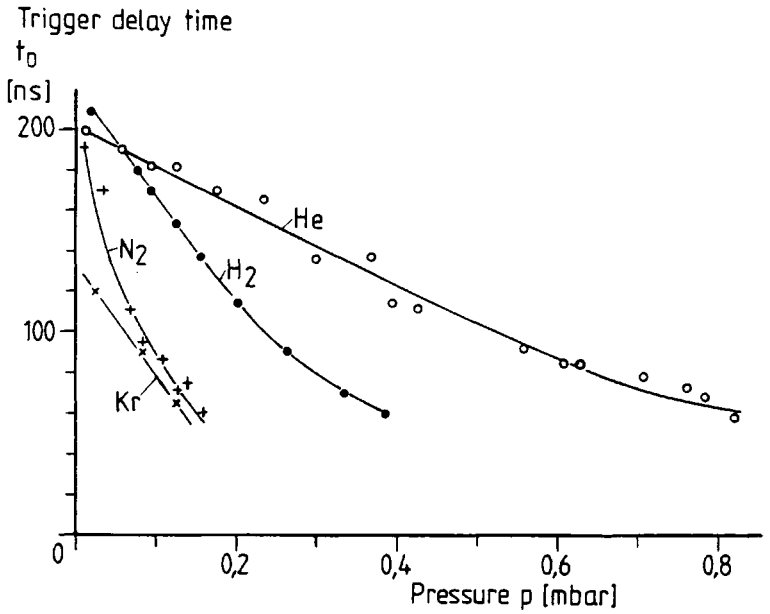
Trigger delay time
t_D
[ns]
200
100
0
He
N_2
H_2
Kr
0,2
0,4
0,6
0,8
Pressure p [mbar]

Fig. 7

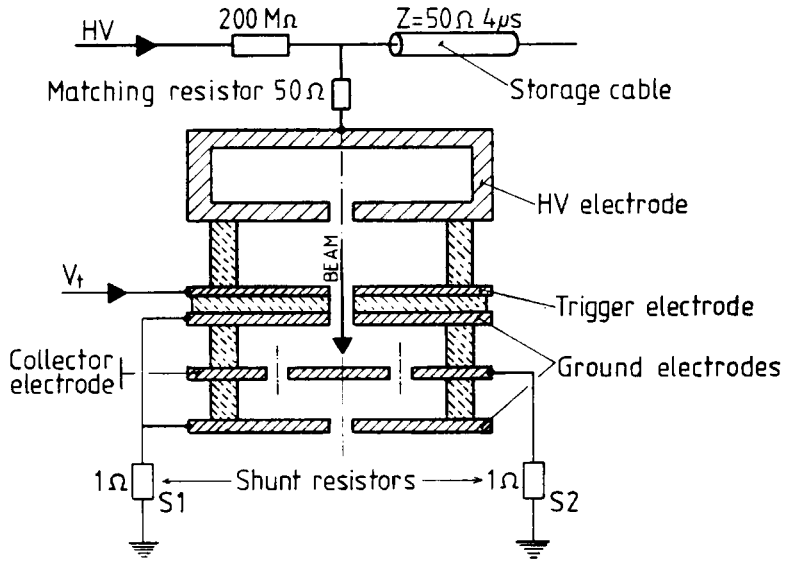
HV
200 MΩ
Z=50 Ω 4μs
Matching resistor 50 Ω
Storage cable
HV electrode
BEAM
V_t
Trigger electrode
Collector electrode
Ground electrodes
1Ω
Shunt resistors
1Ω
S1
S2

a)

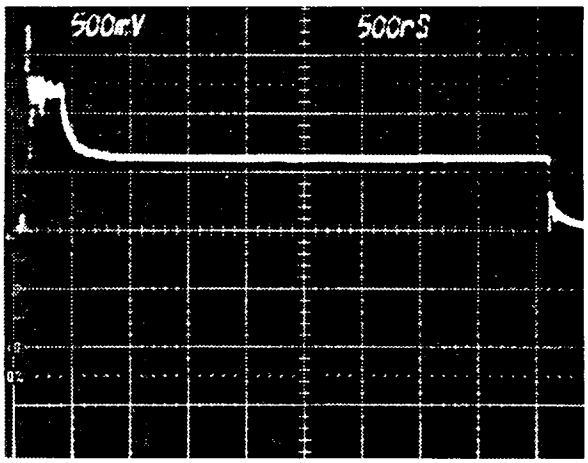
500mV
500nS

b)

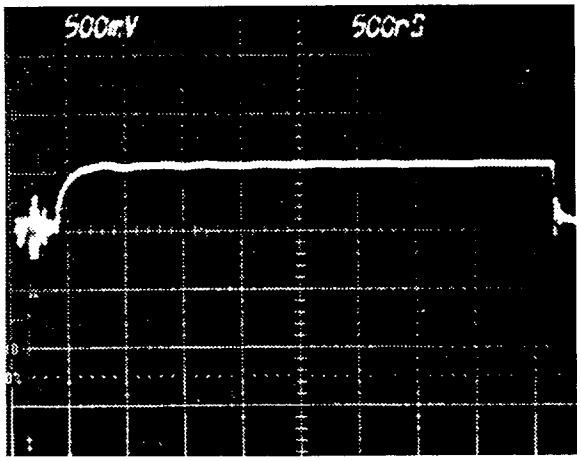
500mV
500nS

c)

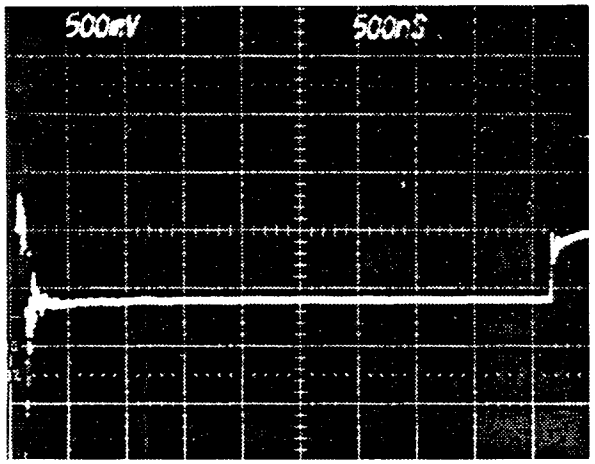
500mV
500nS

d)

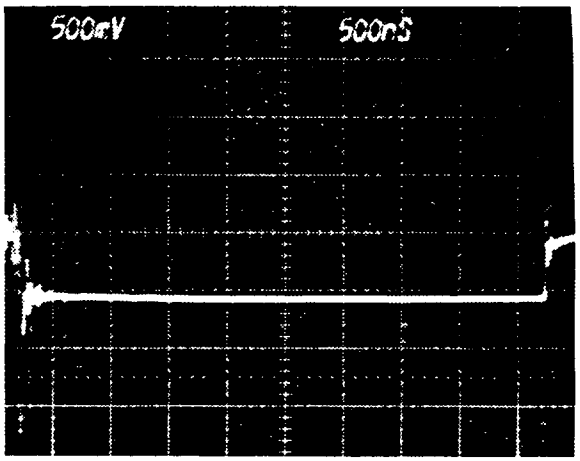
500mV
500nS

e)

Fig. 8

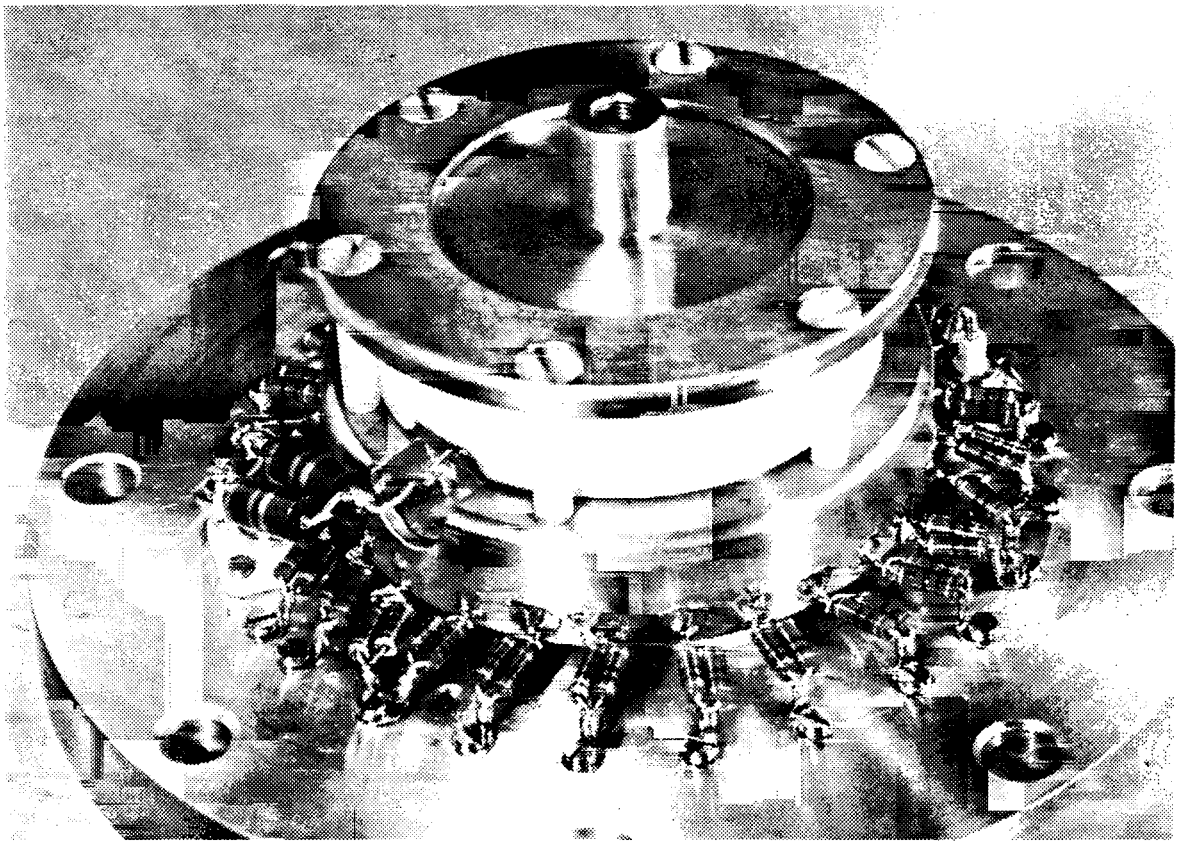

a)

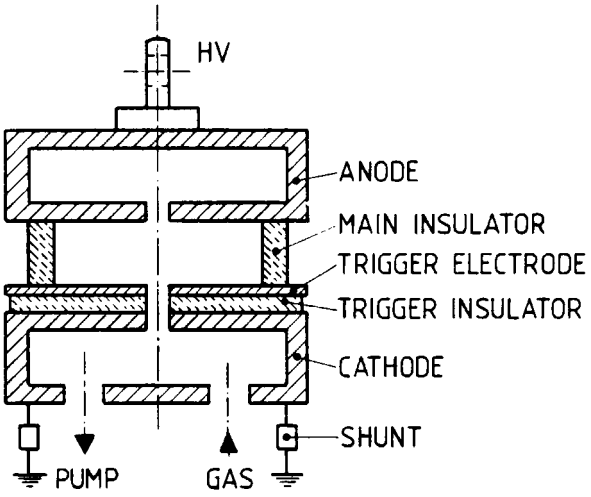
HV
ANODE
MAIN INSULATOR
TRIGGER ELECTRODE
TRIGGER INSULATOR
CATHODE
SHUNT
PUMP
GAS

b)

Fig. 9

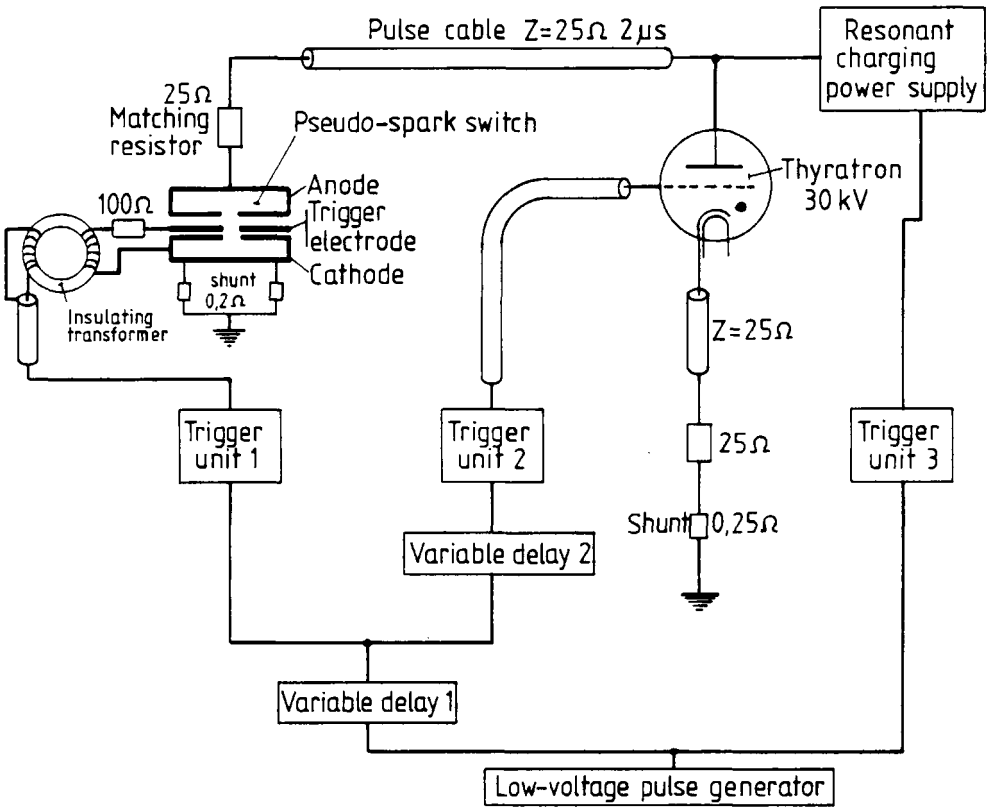

Fig. 10

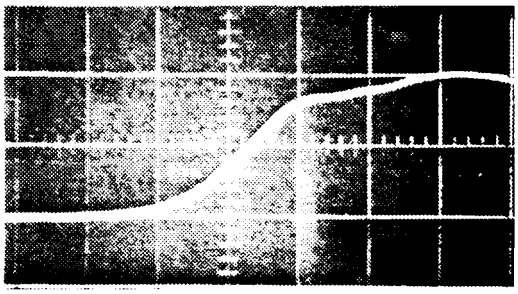

a)

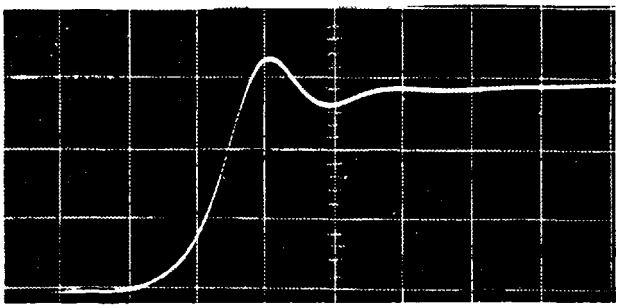

b)

Fig. 11

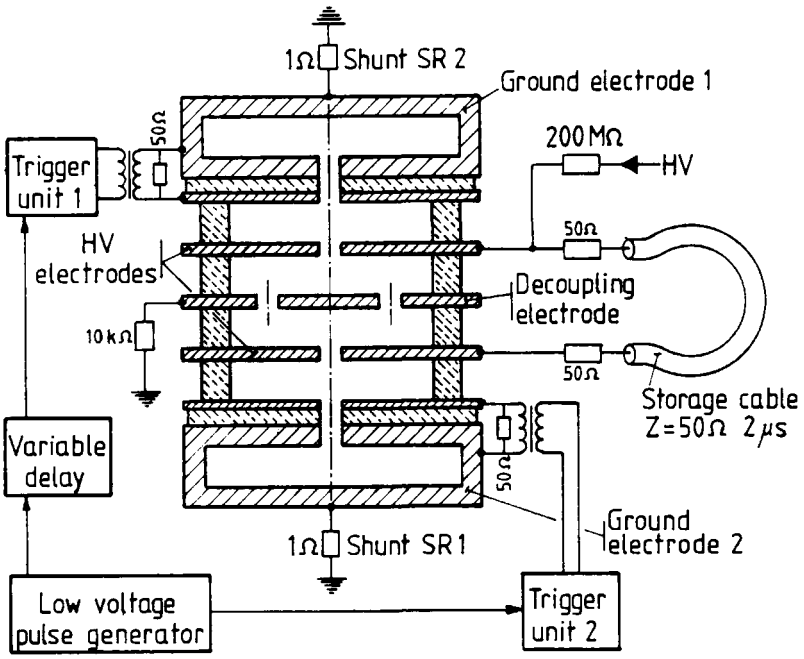
1Ω Shunt SR 2
Ground electrode 1
50Ω
200 MΩ
HV
Trigger unit 1
HV electrodes
50Ω
Decoupling electrode
10 kΩ
50Ω
Storage cable Z=50Ω 2μs
Variable delay
50Ω
Ground electrode 2
1Ω Shunt SR 1
Low voltage pulse generator
Trigger unit 2

a)

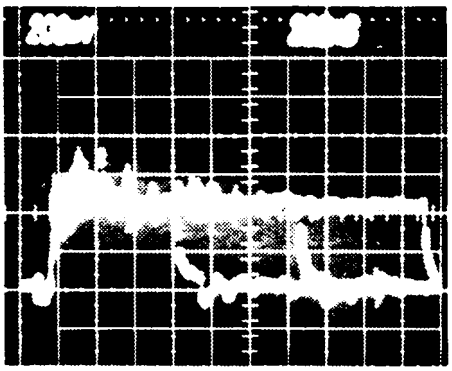

b)

Fig. 12

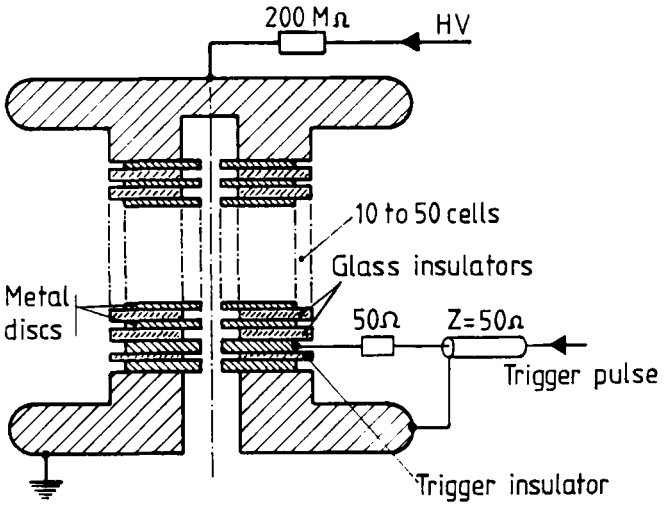
200 MΩ
HV
10 to 50 cells
Glass insulators
Metal discs
50Ω
Z=50Ω
Trigger pulse
Trigger insulator

a)

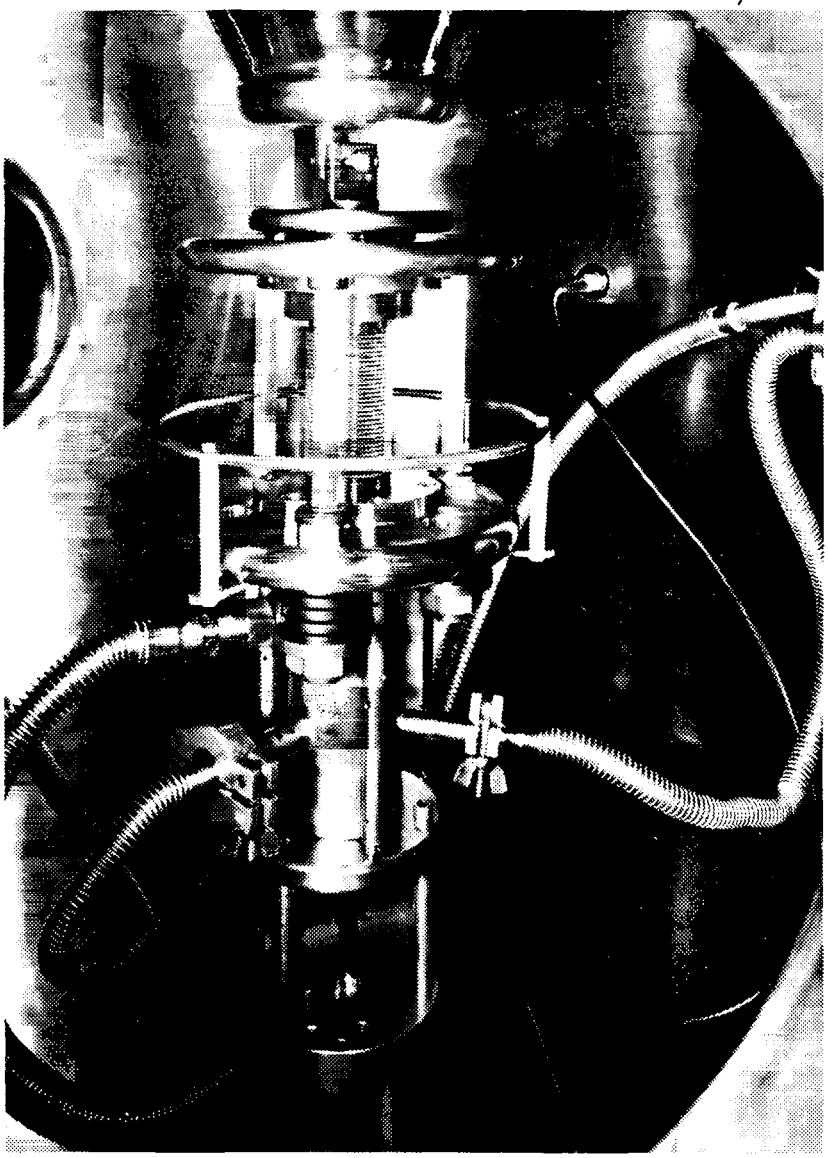

b)

Fig. 13

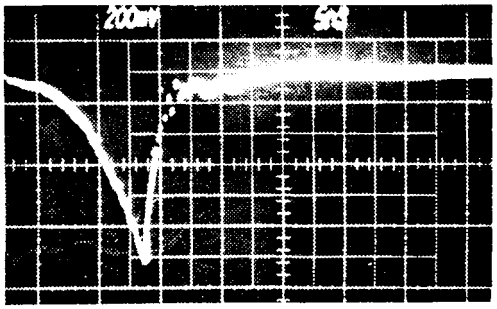

a) Charging voltage -45 kV; 1 A/div.;
max. current 6 A

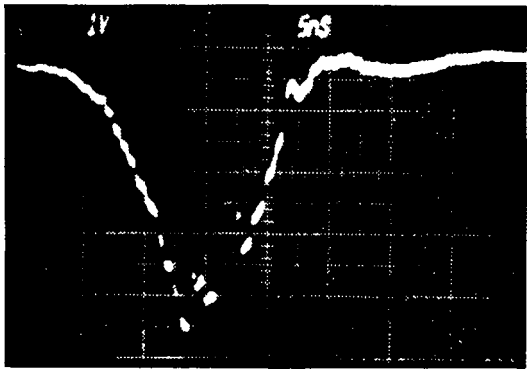

b) Charging voltage -70 kV; 5 A/div.;
max. current 42 A

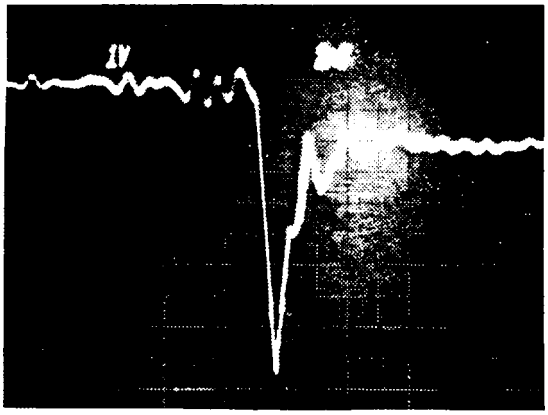

c) Charging voltage -70 kV, 500 A/div.;
max. current 4.5 kA; FWHM 1.5 ns

Fig. 14

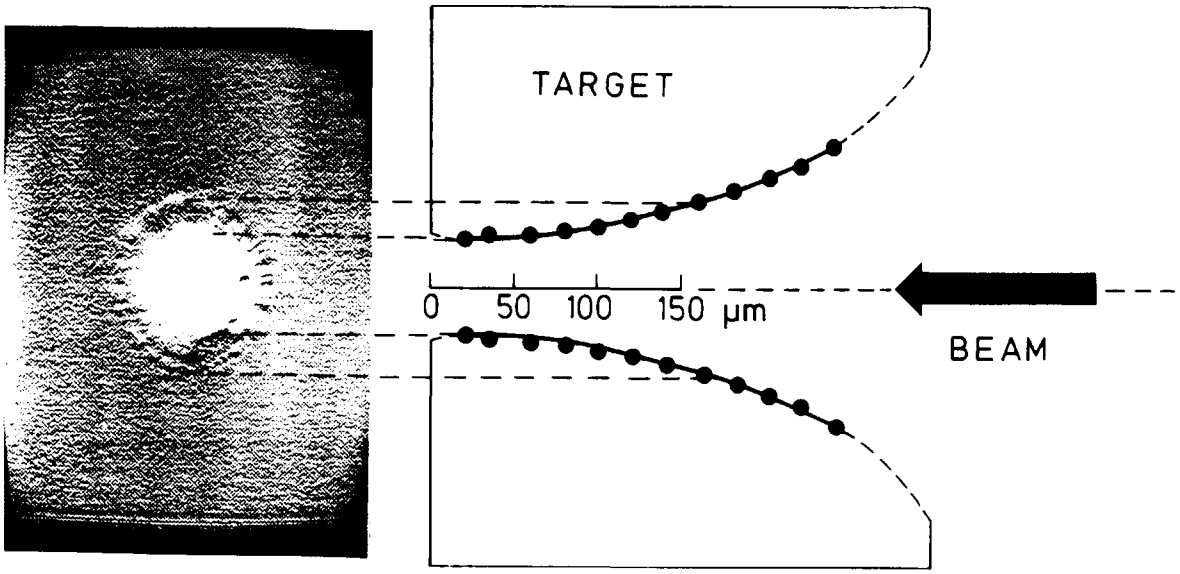

Fig. 15

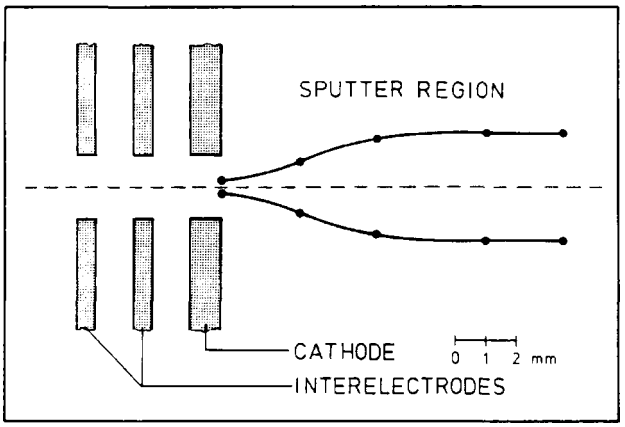

Fig. 16

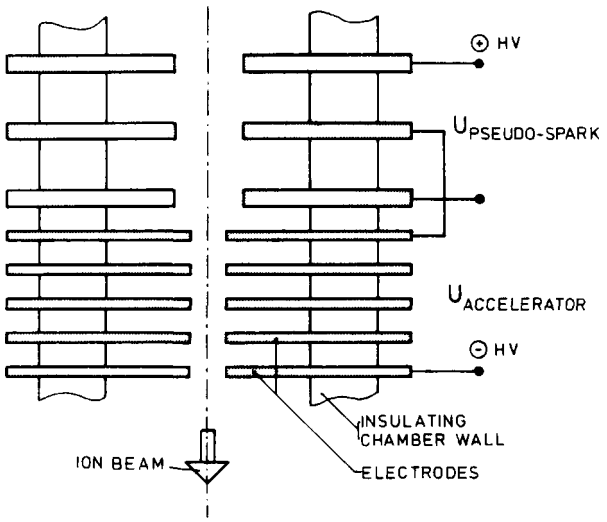

Fig. 17

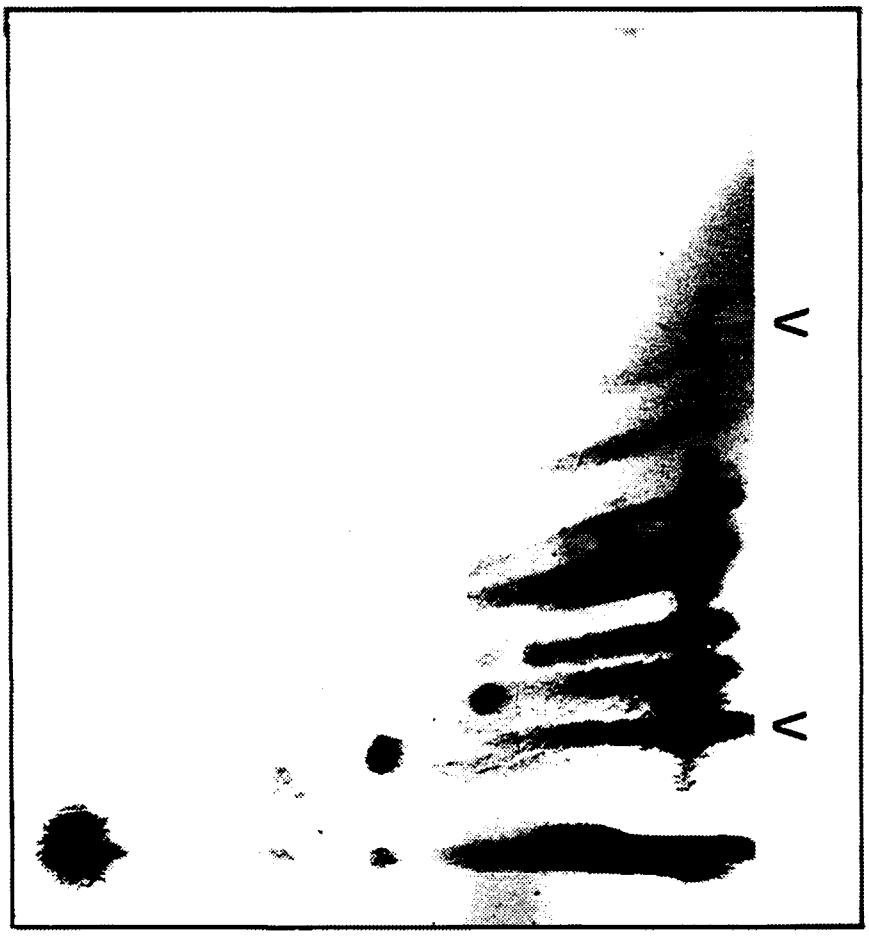

Fig. 18